Journal of Biomedical Research

Cardiomyocyte BMAL1 deficiency worsens obesity-related cardiomyopathy with heightened PINK1/Parkin-linked mitophagy and mitochondrial dysfunction

Tianzi Liu, Xiaoxuan Fan, Nannan Zhang, Yao Wang, Zhiyong Qian, Xiaofeng Hou, Hanwen Zhang, Jiangang Zou

Cite this article as:
Tianzi Liu, Xiaoxuan Fan, Nannan Zhang, Yao Wang, Zhiyong Qian, Xiaofeng Hou, Hanwen Zhang, Jiangang Zou. Cardiomyocyte BMAL1 deficiency worsens obesity–related cardiomyopathy with heightened PINK1/Parkin–linked mitophagy and mitochondrial dysfunction[J]. *Journal of Biomedical Research*, In press. doi: 10.7555/JBR.40.20260012

View online: https://doi.org/10.7555/JBR.40.20260012

Available online at www.jbr-pub.org.cn

Open Access at PubMed Central

Journal of Biomedical Research, 2026 40(0): 1–17

Original Article

JBR

Cardiomyocyte BMAL1 deficiency worsens obesity-related cardiomyopathy with heightened PINK1/Parkin-linked mitophagy and mitochondrial dysfunction

Tianzi Liu[1,△], Xiaoxuan Fan[1,△], Nannan Zhang[2], Yao Wang[1], Zhiyong Qian[1], Xiaofeng Hou[1], Hanwen Zhang[3,4], Jiangang Zou[1,✉]

[1]*Department of Cardiology, The First Affiliated Hospital of Nanjing Medical University, Nanjing, Jiangsu 210029, China;*
[2]*Department of Cardiology, The Affiliated Suzhou Hospital of Nanjing Medical University, Suzhou, Jiangsu 215002, China;*
[3]*Department of Pathophysiology, Nanjing Medical University, Nanjing, Jiangsu 211166, China;*
[4]*Key Laboratory of Jiangsu Province on Targeted Intervention of Cardiovascular Diseases, Nanjing, Jiangsu 211166, China.*

Abstract

Obesity-related cardiomyopathy (OCM) is characterized by pathological cardiac remodeling and progressive functional decline, often accompanied by mitochondrial dysfunction, particularly aberrant mitophagy. The role of the core circadian gene brain and muscle ARNT-like protein 1 (*Bmal1*) in OCM remains unclear. In this study, we employed a high-fat diet (HFD)-induced OCM mouse model, a cardiomyocyte-specific *Bmal1* knockout (*Bmal1*^{CMKO}) model, and a palmitic acid (PA)-induced H9c2 cardiomyocyte injury model to investigate the function of *Bmal1*. *In vivo*, BMAL1 expression was reduced in hearts of HFD mice; HFD-*Bmal1*^{CMKO} mice exhibited exacerbated myocardial hypertrophy, fibrosis, functional impairment, and apoptosis, accompanied by increased expression of the mitophagy-related proteins PINK1, Parkin, and LC3-II. *In vitro*, PA exposure decreased BMAL1 expression, disrupted mitochondrial membrane potential, increased reactive oxygen species generation, and induced excessive mitophagy; these effects were aggravated by *Bmal1* silencing and attenuated by *Bmal1* overexpression, which also improved cell viability. Collectively, these findings indicate that *Bmal1* plays a protective role in OCM, and its downregulation may be a key contributor to obesity-induced cardiac remodeling and dysfunction. Mechanistically, BMAL1 downregulation was accompanied by activation of the PINK1/Parkin signaling and enhanced mitophagy under lipid stress. By restraining excessive mitophagy and preserving mitochondrial function and metabolic homeostasis, *Bmal1* and its associated pathways may represent promising therapeutic targets for OCM.

Keywords: obesity-related cardiomyopathy, heart failure, BMAL1, clock gene, mitophagy, apoptosis

Introduction

Obesity is a chronic metabolic disorder and has become a significant public health concern[1]. It is associated with an elevated risk of several leading causes of death, including cardiovascular disease,

# These authors contributed equally to this work.

✉Corresponding author: Jiangang Zou, E-mail address: jgzou@njmu.edu.cn, ORCID: 0000-0001-5891-6589.

Received: 05 January 2026; Revised: 24 April 2026; Accepted: 30 April 2026;

CLC number: R542.2, Document code: A

The authors reported no conflict of interests.

https://doi.org/10.7555/JBR.40.20260012

metabolic syndrome, type 2 diabetes, and multiple cancers[2]. Obesity can provoke cardiac remodeling and dysfunction, leading to hemodynamic overload, myocardial fibrosis, and reduced ventricular contractility that ultimately culminate in heart failure, pathological changes collectively termed obesity-related cardiomyopathy (OCM)[3]. The Framingham Heart Study demonstrated that the risk of heart failure increases in parallel with body mass index in both sexes[4]. Recent studies have linked the pathogenesis of OCM to adipose-tissue dysfunction, chronic inflammation, metabolic disturbances, oxidative stress, defective mitophagy, mitochondrial Ca^{2+} dysregulation, fibrosis, and endothelial injury [2, 5, 6]; nevertheless, effective therapies to prevent or reverse OCM remain elusive.

Mammals harbor an intrinsic circadian timing system that synchronizes most physiological processes with the 24-hour light–dark cycle[7]. BMAL1 and CLOCK form the core transcriptional activator complex that binds E-box elements to drive rhythmic gene expression[8, 9]. Disruption of this core machinery—especially reduced BMAL1 expression—has emerged as a key driver of metabolic disease and cardiac dysfunction. Recent studies have revealed that BMAL1 expression is markedly decreased in the skeletal muscle of patients with type 2 diabetes, a change closely linked to abnormal mitochondrial metabolism[10]. In addition, BMAL1 modulates mitochondrial dynamics, thereby participating in mitochondrial fission and autophagy and playing a crucial role in the development of dilated cardiomyopathy[11]. Obesity impairs not only the central circadian clock but also the expression of circadian genes in peripheral tissues, thereby exacerbating the risk of metabolic and cardiovascular diseases[12-14].

The myocardium, an exceptionally energy-demanding tissue, is densely packed with mitochondria —occupying roughly one-third of the volume of an adult cardiomyocyte—and derives most of its ATP from mitochondrial oxidative metabolism[15]. Numerous cardiovascular disorders precipitate progressive alterations in mitochondrial architecture and impair mitochondrial function[16, 17]. Mitophagy —the selective autophagic elimination of damaged mitochondria —facilitates organelle turnover, safeguards mitochondrial quality, and prevents the intracellular accumulation of dysfunctional mitochondria[18]. Beyond its roles in metabolic regulation, cell differentiation, and apoptosis, mitophagy has emerged as an important therapeutic target in metabolic heart disease[19, 20]. Experimental evidence shows that stress-induced cardiac mitophagy clears dysfunctional mitochondria, limits reactive oxygen species (ROS)-mediated injury, and thereby reduces the incidence of heart failure[21]. Moreover, mitophagy, dependent on autophagy-related proteins such as ATG7 and the E3 ligase PARKIN, is essential for preserving mitochondrial function and protecting cardiac performance during the early stages of diabetic cardiomyopathy[19]. Nevertheless, it remains unclear whether obesity-driven alterations in cardiac BMALl1 expression contribute to the onset and progression of OCM, and whether this effect is mechanistically linked to the regulation of mitophagy.

Given the above findings, we hypothesized that cardiac BMAL1 downregulation under obesity-induced stress aberrantly activates mitophagy, thereby driving mitochondrial dysfunction, cardiomyocyte apoptosis, and ultimately obesity-related cardiomyopathy.

Materials and methods

Experimental animals

Male C57BL/6J mice (Gempharmatech Co., Ltd., Nanjing, China) were used in this study. The mice were housed in the Laboratory Animal Center of Nanjing Medical University under controlled conditions of constant humidity and temperature, with ad libitum access to water and food. All mice were kept under a strict 12-hour light/dark (LD 12:12) cycle, with lights on at 6:00 a.m. (Zeitgeber time 0, ZT0) and off at 6:00 p.m. (ZT12). At the end of the experiment, mice were anesthetized with 1%–2% isoflurane and euthanized by cervical dislocation.

All experimental procedures were conducted in accordance with the Guide for the Care and Use of Laboratory Animals (8th edition, revised, 2011) published by the U.S. National Institutes of Health. The study protocol was approved by the Laboratory Animal Welfare & Ethics Committee (IACUC) of Nanjing Medical University (Ethics Approval No. 2005052).

Construction of the obesity model

C57BL/6J mice (Gempharmatech Co., Ltd.) were fed a high-fat diet (HF60, Deits Biotechnology, China) starting at 8 weeks of age. Body weight was measured and recorded every 4 weeks for a duration of 12 weeks. After 12 weeks, echocardiography was performed to assess the development of the obesity model.

Construction of cardiomyocyte-specific *Bmal1* knockout mice and cardiac overexpression of BMAL1 in obese mice

Female *Bmal1*$^{flox/flox}$ mice (Jackson Laboratory, Bar Harbor, ME, USA) were bred with male Myh6-cre mice (Jackson Laboratory) to generate *Bmal1*$^{flox/flox}$;α-MHC-Cre$^{+/-}$ mice with Cre-negative *Bmal1*$^{flox/flox}$ littermates used as tamoxifen-treated controls. At 8 weeks of age, both Cre-positive and Cre-negative mice received intraperitoneal tamoxifen (TMX, 50 mg/kg) once daily for 5 consecutive days; cardiomyocyte-specific *Bmal1* knockout was induced specifically in the Cre-positive mice, whereas Cre-negative littermates served as controls to account for any potential effects of TMX administration. Following induction, the mice were fed a high-fat diet (HF60, Deits Biotechnology). Body weight was measured and recorded every 4 weeks for a period of 12 weeks. After 12 weeks, echocardiography was performed to assess the establishment of the model.

Culture and treatment of H9c2 cardiomyoblasts

Rat H9c2 cardiomyoblasts (Zhong Qiao Xin Zhou Biotechnology, Shanghai, China) were cultured in DMEM supplemented with 100 U/mL penicillin, 100 μg/mL streptomycin, and 10% fetal bovine serum. Cells were exposed to either standard medium (the CON group, 5.5 mmol/L D-glucose) or high palmitic acid (PA) medium (the PA group, 400 μmol/L PA) for 24 h. To synchronize intrinsic circadian rhythms, a well-established serum shock method (50% horse serum) was employed to examine the circadian *Bmal1* expression. Detailed synchronization methods are provided in the online ***Supplementary Material***. Recombinant AAV vectors for *Bmal1* overexpression (AAV-*Bmal1*) were obtained from Genechem (Shanghai, China), and the corresponding control vectors were used as controls (AAV-Ctrl). Additionally, *Bmal1* knockdown was achieved using siRNA. After serum starvation for 6–8 hours in serum-free medium, H9c2 cells were transfected with the corresponding adenoviruses for 12 h, followed by culture in either standard or PA medium for an additional 24 h. After serum starvation for 6–8 h in serum-free medium, H9c2 cells were transduced with AAV-*Bmal1* or AAV-Ctrl for 12 h, or transfected with *Bmal1* siRNA or the corresponding negative control for 24 h, followed by culture in either standard medium (5.5 mmol/L D-glucose) or PA-containing medium (400 μmol/L) for an additional 24 h.

Statistical analysis

In this study, all experimental data were expressed as mean ± standard deviation (SD) or percentages. Normality and homogeneity of variance were assessed for all datasets. Differences between the two groups were analyzed using Student's *t*-tests. Comparisons among multiple groups were analyzed using one-way analysis of variance (ANOVA) followed by appropriate post hoc multiple-comparisons tests. For experiments involving two independent variables, two-way ANOVA followed by appropriate post hoc multiple-comparisons tests was used. Correlation analyses were performed using Pearson correlation analysis. Unless otherwise specified, *n* represents the number of independent biological replicates (individual animals). All statistical analyses were performed using GraphPad Prism 9 software, and a *P*-value < 0.05 was considered statistically significant. Additionally, all echocardiographic and histological images were coded prior to analysis, and quantification was conducted in a blinded manner; group codes were unblinded only after completion of statistical analyses.

Results

Reduced expression and disrupted rhythmicity of myocardial BMAL1 in obese mice

To delineate obesity-associated transcriptional changes in the heart, we queried the GEO database with "obesity" AND "heart" and analyzed dataset GSE264313, which compares obese and control groups. We identified 2 070 differentially expressed genes, including 1 372 upregulated and 698 downregulated genes (***Fig. 1A***). Focusing on core circadian regulators, *Bmal1* exhibited the most pronounced changes, showing marked downregulation in obese mouse hearts, whereas *Clock* expression remained unchanged between groups (***Fig. 1B***). These findings implicate *Bmal1* as a key node linking obesity to cardiac circadian dysregulation and prioritize it for mechanistic investigation.

We next examined *Bmal1* expression across circadian time points in the hearts of obese mice. Quantitative PCR analysis of cardiac RNA revealed a distinct circadian pattern of *Bmal1* expression in the control group (CD mice), with expression peaking at ZT0 (06:00 AM) and ZT24 (06:00 AM the following day), and reaching its nadir at ZT12 (06:00 PM) (***Fig. 1C***). In contrast, high-fat diet (HFD)-fed obese mice exhibited significantly reduced *Bmal1* expression across all time points (ZT0, ZT12, ZT24), accompanied by a complete loss of circadian rhythmicity, while *Clock* mRNA levels remained

unchanged (***Fig. 1C***). This downregulation was confirmed at the protein level by Western blot analysis (***Fig. 1D*** *and* ***1E***) and further validated by immunohistochemical staining, which showed a significantly reduced BMAL1-positive area in the myocardium of HFD mice compared with control mice (***Fig. 1F*** and ***1G***).

Physiological assessments indicated that HFD mice had increased body weight, elevated fasting blood glucose levels, and impaired glucose tolerance compared with the CD group (***Supplementary Fig. 1A–1C***). Representative echocardiographic images, including M-mode, pulsed-wave Doppler, and tissue Doppler imaging, are shown in ***Fig. 1H***. Echocardiographic analysis further revealed impaired diastolic function, as indicated by a increased E/e′ ratio, in obese mice. However, no statistically significant differences were observed between the two groups in terms of left ventricular ejection fraction (LVEF) or fractional shortening (LVFS) (***Fig. 1I***). Serum BNP levels were significantly higher in the HFD group than in the control group, whereas no significant difference in ANP levels was observed between the two groups (***Fig. 1J***). These findings suggest the presence of cardiac stress in obese mice.

Cardiomyocyte-specific knockout of *Bmal1* exacerbates cardiac hypertrophy, fibrosis, lipid accumulation, and diastolic dysfunction in obese mice

To investigate the role of BMAL1 in cardiac pathophysiology under obese conditions, we generated mice with cardiomyocyte-specific *Bmal1* knockout (*Bmal1*^{CMKO}). The experimental workflow is illustrated in ***Fig. 2A***.

Echocardiographic assessment showed impaired diastolic function in obese mice, characterized by a significantly elevated E/e′ ratio, prolonged isovolumic relaxation time (IVRT), and a reduced E/A ratio(***Fig. 2B***, ***2C***, and ***Supplementary Fig. 2A***). Systolic function remained preserved, with no significant difference in LVEF or LVFS across groups. Structural measurements indicated significant thickening of the interventricular septum (IVST), left ventricle anterior wall in diastole and systole (LVAWd/s), and left ventricle posterior wall in diastole (LVPWd) in HFD-fed mice. These changes were further accentuated in HFD-fed *Bmal1*^{CMKO} mice, indicating that

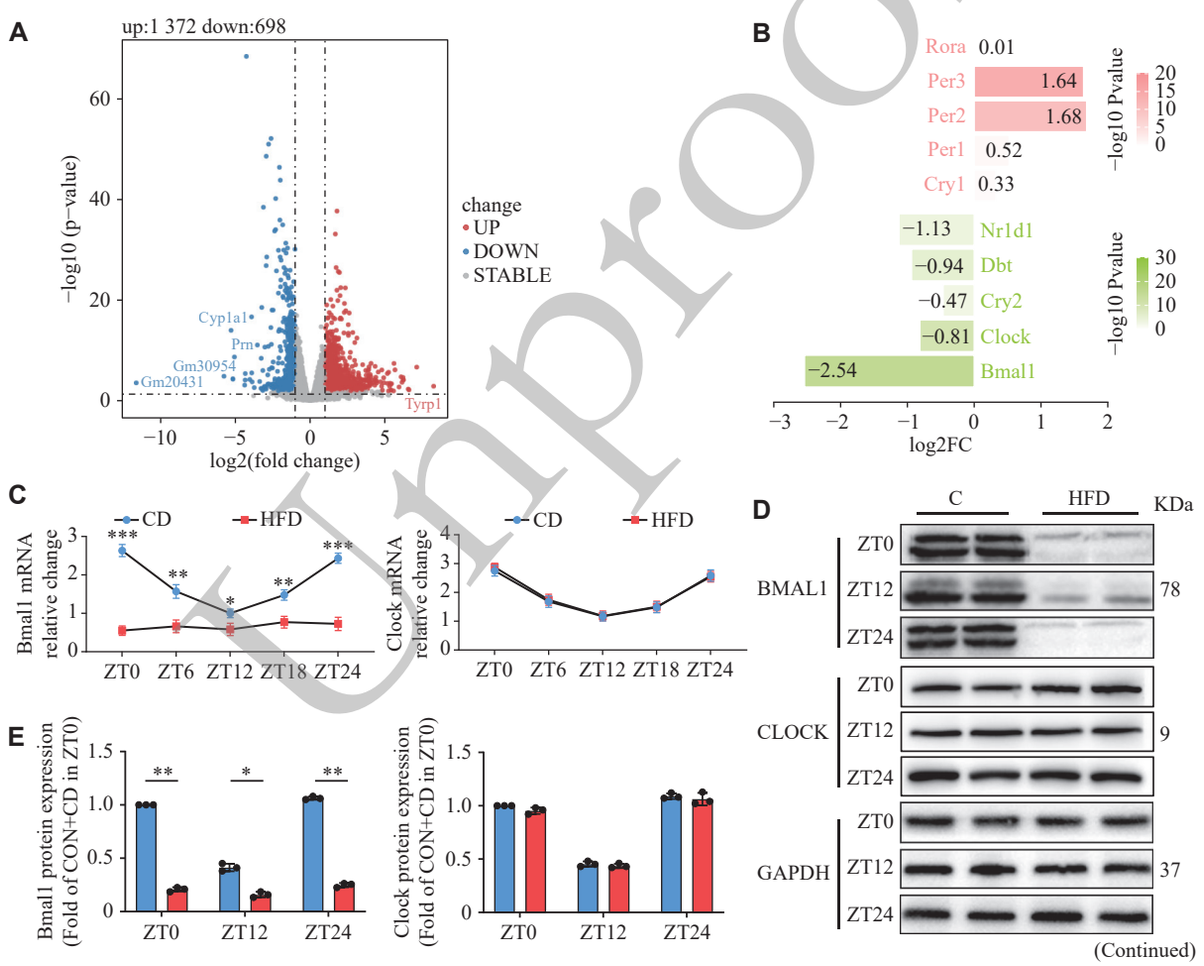

(Continued)

(Continued)

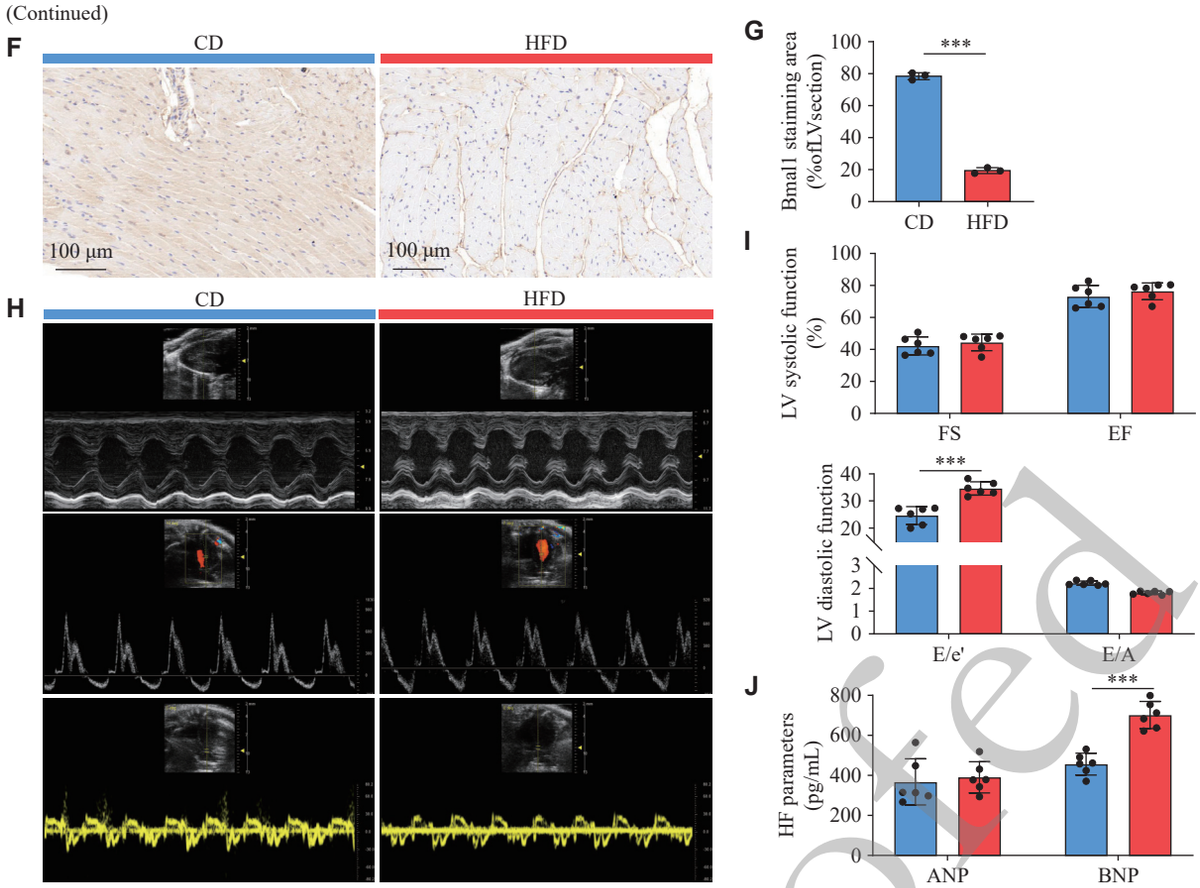

Fig. 1 **High-fat diet disrupts cardiac BMAL1 rhythmicity and impairs diastolic function in obese mice.** A: Volcano plot of differentially expressed genes in hearts from obese versus control mice in GEO dataset GSE264313, identifying 1372 upregulated and 698 downregulated genes. Red and blue dots denote upregulated and downregulated genes, respectively. B: Log_2(fold change [FC]) of core circadian clock genes in the same dataset, highlighting *Bmal1* as the most strongly suppressed regulator in obese hearts, whereas *Clock* expression is unchanged. C: Temporal profile of cardiac *Bmal1* and *Clock* mRNA levels measured by qPCR in CD and HFD mice across the light–dark cycle (ZT0, ZT6, ZT12, ZT18, and ZT24; $n = 6$ per time point per group). D: Western blot of cardiac BMAL1 and CLOCK protein levels across different ZT points; GAPDH was used as a loading control. E: Quantification of BMAL1 and CLOCK protein expression normalized to CD at ZT0 ($n = 3$ per group). F: Representative immunohistochemical staining of BMAL1 in left ventricular sections. Scale bars, 100 μm. G: Quantification of BMAL1-positive staining area (% of LV section; $n = 3$ per group). H: Representative echocardiographic images showing M-mode, pulsed-wave Doppler, and tissue Doppler imaging. I: Quantification of echocardiographic parameters: LV systolic function (fractional shortening [FS] and ejection fraction [EF]); LV diastolic function (E/e′ and E/A ratios). J: Plasma levels of heart failure markers (ANP and BNP levels; $n = 6$ per group). Data are presented as mean ± standard error (SD); each dot represents one mouse (biological replicate). For panels C and E, statistical analysis was performed using two-way ANOVA followed by Sidak's multiple-comparisons test. For panels G, I, and J, comparisons between two groups were performed using an unpaired two-tailed Student's t test. Statistical significance is indicated as $^{*}P < 0.05$, $^{**}P < 0.01$, and $^{***}P < 0.001$. Abbreviations: ANP, atrial natriuretic peptide; BNP, B-type natriuretic peptide; CD, control diet; HFD, high-fat diet; LV, left ventricle; ZT, Zeitgeber time (ZT0 corresponds to lights on at 06:00).

cardiomyocyte-specific *Bmal1* knockout potentiates obesity-induced cardiac remodeling (***Table 1***).

Hematoxylin and Eosin (H&E) staining demonstrated pathological cardiac hypertrophy in obese mice, which was further aggravated by *Bmal1* deficiency (***Fig. 2D***). Oil Red O staining of frozen heart sections revealed prominent lipid droplet accumulation in the myocardium of obese mice, with a marked increase in lipid deposition upon *Bmal1* knockout (***Fig. 2E*** and ***2H***). Masson staining showed that *Bmal1* deficiency significantly worsened cardiac fibrosis in obese mice, as evidenced by an increased fibrotic area in the myocardium (***Fig. 2F*** and ***2I***). Wheat germ agglutinin (WGA) staining revealed myocardial hypertrophy, with an enlarged cardiomyocyte cross-sectional area in obese mice, which was further increased in cardiomyocyte-specific *Bmal1* knockout mice (***Fig. 2G*** and ***2J***).

Cardiomyocyte-specific *Bmal1* knockout aggravates obesity-induced mitochondria-mediated cardiomyocyte apoptosis

To elucidate the impact of HFD and cardiomyocyte-specific *Bmal1* knockout on

myocardial apoptosis, TUNEL staining was performed on cardiac tissue sections. Increased cardiomyocyte apoptosis was observed in both HFD-fed mice (HFD-*Bmal1*$^{fl/fl}$) and cardiomyocyte-specific *Bmal1* knockout mice fed a control diet (CD-*Bmal1*^{CMKO}), with a further significant elevation in apoptosis in *Bmal1*-knockout mice subjected to HFD (HFD-*Bmal1*^{CMKO}) (***Fig. 3A*** and ***3C***).

Transmission electron microscopy (TEM) was employed to evaluate mitochondrial ultrastructural alterations. By measuring the number of mitochondria and conducting mitochondrial morphology scoring, the structural differences in mitochondria were assessed. Mice in both the HFD-*Bmal1*$^{fl/fl}$ and CD-*Bmal1*^{CMKO} groups exhibited signs of mitochondrial damage, including reduced mitochondrial density, pronounced swelling, increased cross-sectional area, and disrupted or fragmented cristae (***Fig. 3B*** and ***3D–3F***). These pathological changes were markedly more severe in the HFD-*Bmal1*^{CMKO} group, indicating a synergistic effect between *Bmal1* deficiency and HFD-induced metabolic stress.

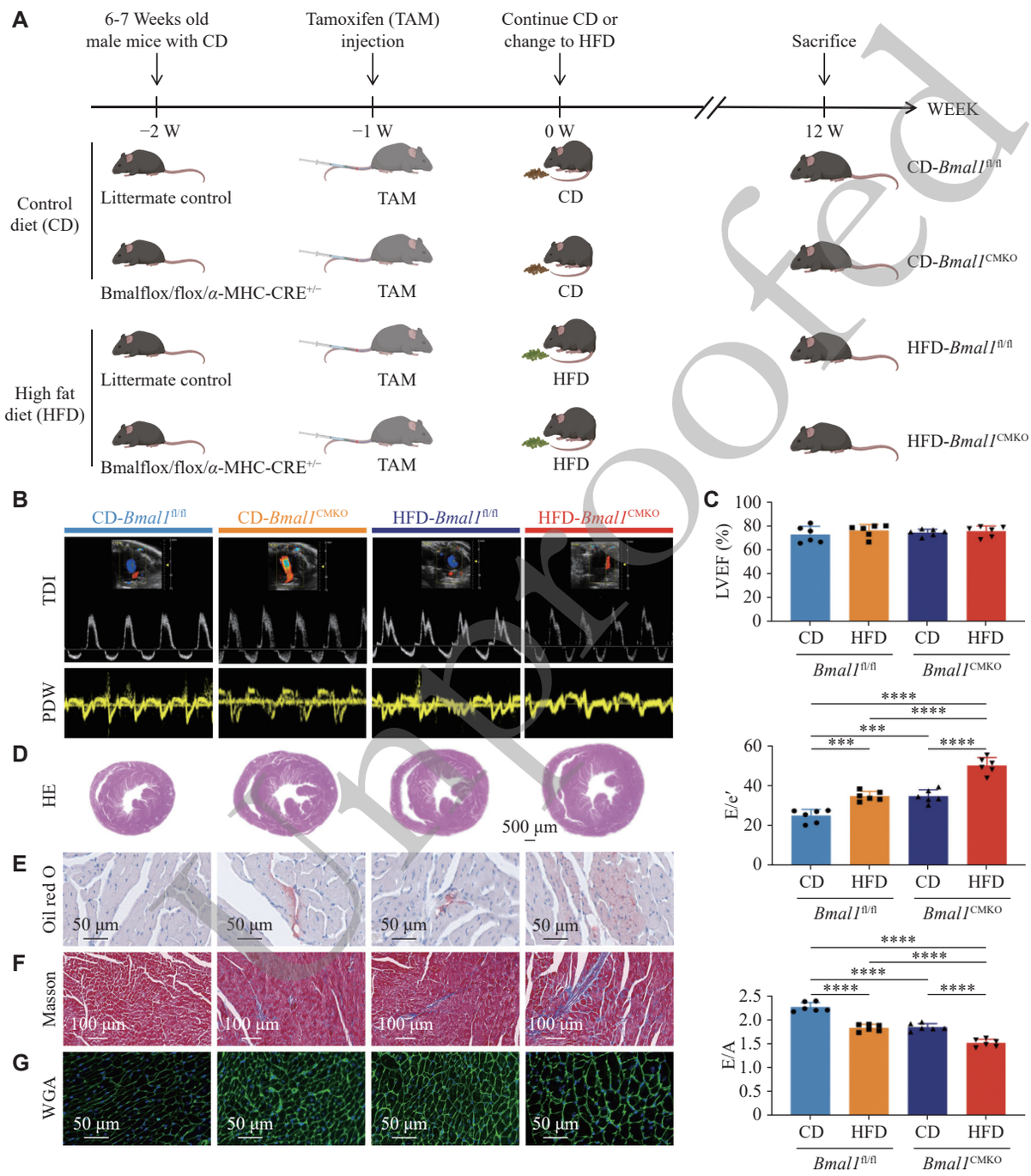

(Continued)

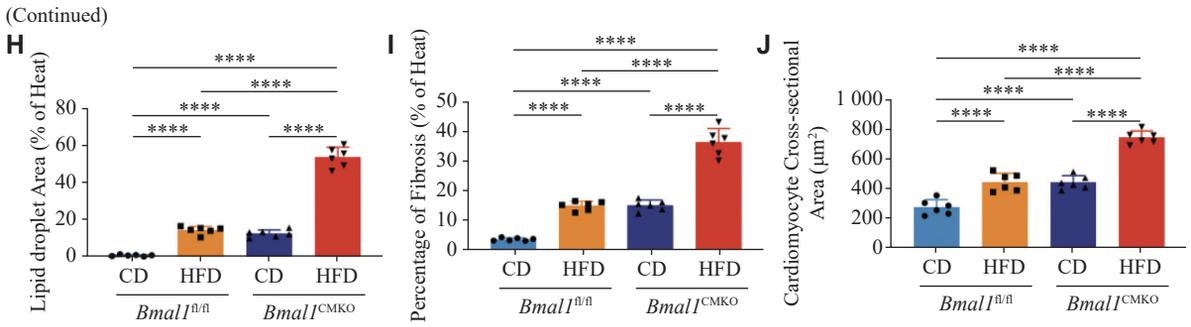

Fig. 2 **Cardiomyocyte-specific *Bmal1* knockout exacerbates cardiac remodeling and diastolic dysfunction in obese mice.** A: Experimental design. Male C57BL/6J mice (6–7 weeks old) were treated with tamoxifen (TAM) to induce cardiomyocyte-specific *Bmal1* knockout (*Bmal1*^{CMKO}) and subsequently fed either a control diet (CD) or a high-fat diet (HFD) for 12 weeks. Mice were divided into four groups: CD-*Bmal1*$^{fl/fl}$, HFD-*Bmal1*$^{fl/fl}$, CD-*Bmal1*^{CMKO}, and HFD-*Bmal1*^{CMKO}. B: Representative transthoracic echocardiographic Doppler recordings, including pulsed-wave Doppler of mitral inflow (top) and tissue Doppler imaging of the mitral annulus (bottom), used to derive diastolic indices. C: Quantification of echocardiographic parameters: left ventricular ejection fraction (LVEF), E/e′ ratio, E/A ratio (n = 6 per group). D: Representative hematoxylin and eosin (H&E)-stained transverse sections of hearts from the indicated groups. Scale bars, 500 μm. E: Oil Red O staining of frozen sections showing myocardial lipid droplet accumulation. Scale bars, 50 μm. F: Masson's trichrome staining revealed interstitial and perivascular fibrosis, which was markedly increased in the HFD-*Bmal1*^{CMKO} group. Scale bars, 100 μm. G: Wheat germ agglutinin (WGA) staining outlines cardiomyocyte membranes and enables assessment of cross-sectional area. Scale bars, 50 μm. H: Quantification of lipid droplet area (% of heart; n = 6 per group). I: Quantification of fibrotic area (% of heart; n = 6 per group). J: Quantification of cardiomyocyte cross-sectional area (μm²; n = 6 per group). Data are presented as mean ± standard error (SD); each dot represents one mouse (biological replicate). Statistical analyses were performed using one-way ANOVA with appropriate post hoc tests; $^{***}P < 0.001$, and $^{****}P < 0.0001$.

Table 1 **Comparison of weight and echocardiographic parameters in each group.**

Variables	CD-*Bmal1*$^{fl/fl}$	HFD-*Bmal1*$^{fl/fl}$	CD-*Bmal1*^{CMKO}	HFD-*Bmal1*^{CMKO}
Weight				
0w(g)	25.35 ± 0.64	25.98 ± 0.69	26.15 ± 0.69	25.88 ± 0.43
4w(g)	27.97 ± 0.49	29.95 ± 0.33**	28.9 ± 0.57*	31.9 ± 0.53##
8w(g)	29.98 ± 0.51	35.35 ± 0.58**	30.65 ± 0.44*	38.15 ± 0.61##
12w(g)	30.85 ± 0.33	39.18 ± 0.51**	31.27 ± 0.18*	41.42 ± 0.46##
Echocardiography				
LVAWs (mm)	1.59 ± 0.04	1.71 ± 0.03**	1.69 ± 0.03**	2.12 ± 0.06##
LVAWd (mm)	1.05 ± 0.04	1.13 ± 0.04*	1.14 ± 0.04*	1.34 ± 0.07##
LVPWs (mm)	1.46 ± 0.03	1.52 ± 0.02**	1.50 ± 0.03*	1.71 ± 0.03##
LVPWd (mm)	0.90 ± 0.02	0.98 ± 0.07**	0.99 ± 0.05**	1.20 ± 0.05##
LV mass (g)	0.15 ± 0.01	0.19 ± 0.02*	0.19 ± 0.02*	0.26 ± 0.03##
E/A	2.24 ± 0.10	1.81 ± 0.07**	1.82 ± 0.07**	1.50 ± 0.08##
E/e’	24.72 ± 3.27	34.64 ± 2.44**	34.55 ± 3.27**	49.95 ± 4.04##
IVRT (ms)	13.92 ± 1.55	16.86 ± 1.22*	17.17 ± 0.97*	24.16 ± 2.34##
LVFS (%)	42.30 ± 5.68	44.38 ± 5.18	43.96 ± 2.23	43.62 ± 2.36
LVEF (%)	73.12 ± 6.95	76.36 ± 5.28	74.78 ± 2.79	75.74 ± 4.51
CO (mL/min)	25.24 ± 4.87	25.79 ± 4.42	21.21 ± 1.99	23.39 ± 4.45

Data are presented as mean ± standard error (SD) (n = 6 mice per group). Statistical significance is indicated as $^{*}P < 0.05$ and $^{**}P < 0.01$ *vs.* the CD-*Bmal1*$^{fl/fl}$ group; $^{\#}P < 0.05$ and $^{\#\#}P < 0.01$ *vs.* the HFD-*Bmal1*$^{fl/fl}$ group. Body weight over time was analyzed using two-way repeated-measures ANOVA followed by Sidak’s multiple-comparisons test. Echocardiographic parameters were analyzed using two-way ANOVA followed by Sidak’s multiple-comparisons test to assess the effects of diet and genotype. Echocardiographic parameters include left ventricular anterior wall thickness in systole (LVAWs) and diastole (LVAWd), posterior wall thickness in systole (LVPWs) and diastole (LVPWd), left ventricular internal diameter in systole (LVIDs) and diastole (LVIDd), E/A ratio, E/e’ ratio, isovolumic relaxation time (IVRT), fractional shortening (LVFS), left ventricular ejection fraction (LVEF), and cardiac output (CO). Abbreviations: CD, control diet; HFD, high-fat diet.

Furthermore, in the myocardial cells of both the HFD-fed mice and the CD-*Bmal1*^{CMKO} group mice, there was an increase in the degree of autophagy. The number of mitophagic events and the proportion of mitochondria within autophagic structures were significantly increased, demonstrating that either HFD feeding or

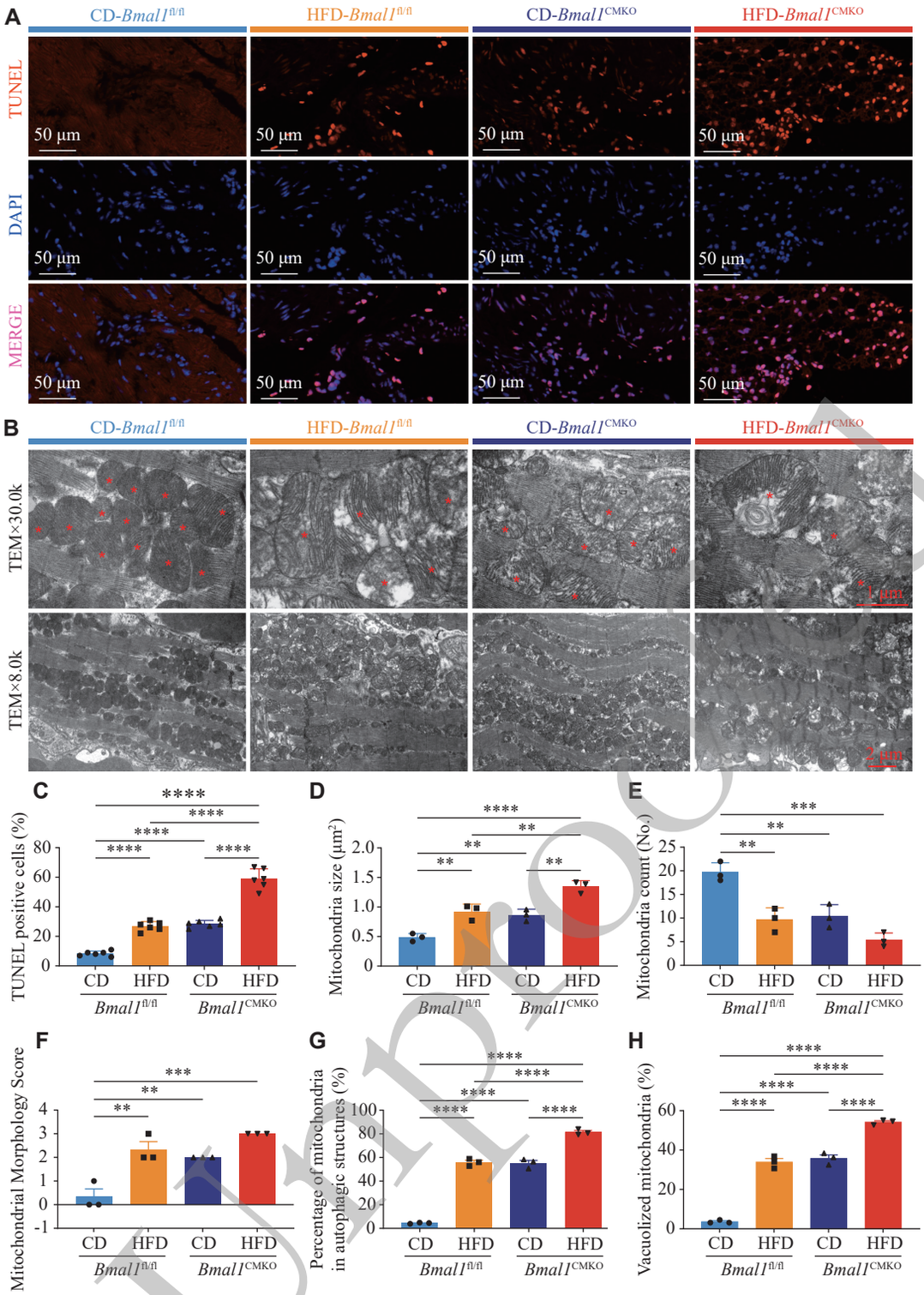

Fig. 3 **Cardiomyocyte-specific *Bmal1* knockout aggravates obesity-induced mitochondrial damage and apoptosis.** A: Representative TUNEL staining of left-ventricular sections from CD-*Bmal1*$^{fl/fl}$, HFD-*Bmal1*$^{fl/fl}$, CD-*Bmal1*^{CMKO} and HFD-*Bmal1*^{CMKO} mice. Nuclei were counterstained with DAPI; merged images show apoptotic cardiomyocytes. Scale bar, 50 μm. B: Transmission electron microscopy (TEM) images showing mitochondrial ultrastructure. Red asterisks indicate swollen or disrupted mitochondria, with HFD-*Bmal1*^{CMKO} hearts displaying extensive mitochondrial damage. Scale bars, 1 μm (top) and 2 μm (bottom) (n = 3 per group). C-H: Quantification of TUNEL-positive cardiomyocytes (C), mitochondrial cross-sectional area (D), mitochondrial number per field (E), mitochondrial morphology score (F), percentage of mitochondria contained within autophagic structures (G), and proportion of vacuolized mitochondria (H). Data are presented as mean ± standard error (SD); each dot represents one mouse (biological replicate). For panels C and H–J, statistical analysis was performed using two-way ANOVA followed by Sidak's multiple-comparisons test to assess the effects of genotype and diet. Statistical significance is indicated as $^{*}P < 0.05$, $^{**}P < 0.01$, and $^{***}P < 0.001$ and $^{****}P < 0.0001$. Abbreviations: CD, control diet; HFD, high-fat diet; CMKO, cardiomyocyte-specific knockout.

cardiomyocyte-specific *Bmal1* deletion activates mitophagy (***Fig. 3G*** and ***3H***). Under combined HFD and *Bmal1* knockout conditions, mitophagy was further exacerbated in the HFD-*Bmal1*^{CMKO} group.

High-fat stimulation disrupts *Bmal1* expression and enhances apoptosis and mitophagy in cardiomyocytes

To establish an *in vitro* model of lipotoxic cardiomyopathy, H9c2 cardiomyoblasts were cultured in high-fat medium supplemented with PA. Oil Red O staining confirmed prominent lipid droplet accumulation in PA-exposed cardiomyocytes (***Supplementary Fig. 3A***). Compared with controls, *Bmal1* mRNA levels were significantly reduced at all circadian time points following serum shock in PA-treated cells (***Fig. 4A***). In contrast, another core clock gene, *Clock*, showed robust rhythmic expression, peaking at ZT0/24 and reaching a nadir at ZT12; PA treatment did not significantly alter its expression

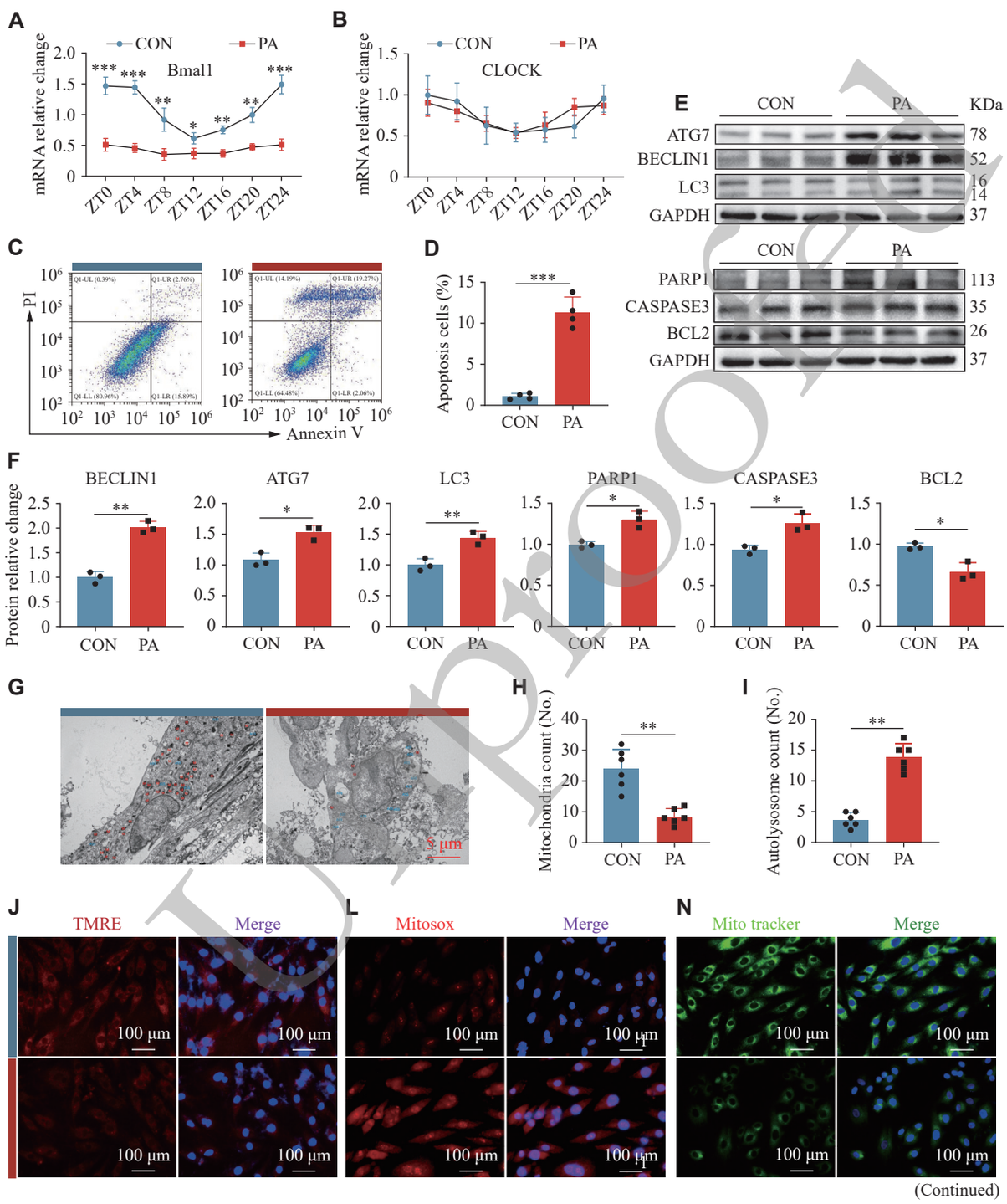

(Continued)

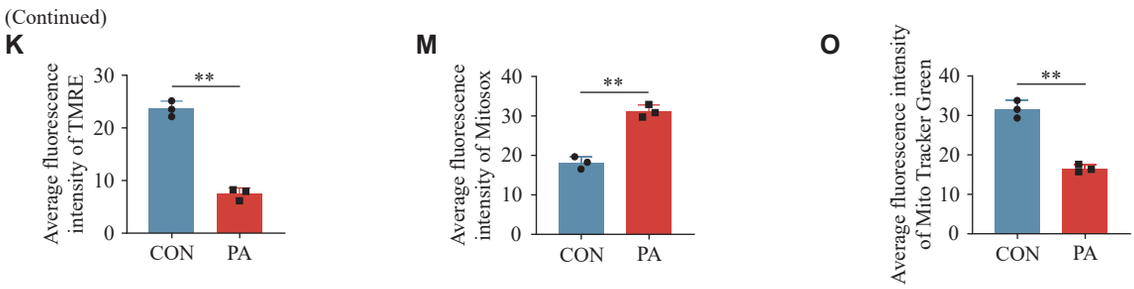

Fig. 4 **Palmitic acid induces apoptosis, enhances mitophagy, and impairs mitochondrial function in cardiomyocytes.** A: Temporal profile of cardiac *Bmal1* mRNA levels measured by qPCR in H9c2 cells cultured in standard medium (CON) or PA-containing medium (PA, 400 μmol/L) for 24 h, followed by serum-shock synchronization with 50% horse serum for 2 h; cells were harvested at ZT0, ZT4, ZT8, ZT12, ZT16, ZT20, and ZT24 for qPCR analysis (n = 3 per time point per group). B: Temporal profile of cardiac *Clock* mRNA levels in H9c2 cells treated as in panel A (n = 3 per time point per group). C: Representative flow cytometry plots of Annexin V/PI staining in H9c2 cells cultured in standard medium (CON) or treated with PA (400 μmol/L) for 24 h. D: Quantification of apoptotic cell percentage from (C) (n = 3 per group). E: Representative western blots of ATG7, BECLIN1, LC3, PARP1, CASPASE3, and BCL2 in H9c2 cells cultured in standard medium (CON) or treated with PA (400 μmol/L) for 24 h. GAPDH served as the loading control. F: Quantification of protein levels from (E), normalized to the CON group (n = 3 per group). G: Representative transmission electron microscopy images of H9c2 cells cultured in standard medium (CON) or treated with PA (400 μmol/L) for 24 h; red and blue arrowheads indicate mitochondria and autolysosomes, respectively. Scale bars, 5 μm. H: Quantification of mitochondrial number per field from TEM images (n = 3 per group). I: Quantification of autolysosome count per field from TEM images (n = 3 per group). J: Representative TMRE staining of H9c2 cells cultured in standard medium (CON) or treated with PA (400 μmol/L) for 24 h. DAPI was used for nuclear counterstaining. K: Quantification of average fluorescence intensity of TMRE from panel J (n = 3 per group). L: Representative MitoSOX staining of H9c2 cells cultured in standard medium (CON) or treated with PA (400 μmol/L) for 24 h. DAPI was used for nuclear counterstaining. M: Quantification of average fluorescence intensity of MitoSOX (L) (n = 3 per group). N: Representative MitoTracker Green staining of H9c2 cells cultured in standard medium (CON) or treated with PA (400 μmol/L) for 24 h. DAPI was used for nuclear counterstaining. O: Quantification of average fluorescence intensity of MitoTracker (N) (n = 3 per group). Data are presented as mean ± standard error (SD); each dot represents one mouse (biological replicate). For panels A and B, statistical analysis was performed using two-way ANOVA followed by Sidak's multiple-comparisons test. For panels D, F, H, I, K, M, and O, comparisons between two groups were performed using an unpaired two-tailed Student's t test. Statistical significance is indicated as $^{**}P < 0.01$, and $^{***}P < 0.001$ vs. the CON group. Abbreviations: CON, control; PA, palmitic acid; ZT, Zeitgeber time; ATG7, autophagy related 7; BCL2, B-cell lymphoma 2; LC3, microtubule-associated protein 1 light chain 3; PARP1, poly(ADP-ribose) polymerase 1; PI, propidium iodide; ROS, reactive oxygen species; TEM, transmission electron microscopy; TMRE, tetramethylrhodamine ethyl ester.

amplitude (***Fig. 4B***).

Flow cytometry (FACS) analysis revealed a higher apoptotic rate in the PA group than in controls (***Fig. 4C*** and ***4D***). Consistent with these findings, CCK-8 assays showed a dose-dependent reduction in cell viability: at 0.4 mmol/L PA, viability declined to approximately 80% of control levels, and at 0.5 mmol/L PA, to around 50% (***Supplementary Fig. 3B***). PA treatment markedly increased the expression of autophagy-related proteins (BECLIN 1, ATG7, and LC3, used to evaluate autophagosome formation) and apoptosis markers (cleaved PARP1 and cleaved Caspase-3, used to assess apoptosis activation), while the anti-apoptotic protein BCL-2 (a key regulator of the mitochondrial apoptotic pathway) was notably downregulated (***Fig. 4E*** and ***4F***).

TEM imaging demonstrated a substantial decrease in mitochondrial number and a concurrent increase in autolysosomes in PA-treated cells, indicating enhanced mitophagy (***Fig. 4G–4I*** and ***Supplementary 3C***). These results suggest that lipid overload leads to downregulation of the core circadian gene *Bmal1*, alongside increased apoptosis and mitophagic activity in cardiomyocytes.

To further assess mitochondrial dysfunction, TMRE staining was performed to measure mitochondrial membrane potential (MMP, ΔΨm). Both fluorescence microscopy and microplate-based quantification showed a significant reduction in ΔΨm following PA exposure (***Fig. 4J*** and ***4K***). MitoSOX staining revealed that PA stimulation elicited excessive ROS production, accompanied by a marked decline in intracellular ATP levels (***Fig. 4L, 4M, and Supplementary 3D***). MitoTracker Green staining showed a pronounced reduction in mitochondrial content in cardiomyocytes following lipid overload (***Fig. 4N*** and ***4O***).

Overexpression of *Bmal1* mitigates PA-induced apoptosis, excessive mitophagy, and mitochondrial dysfunction in H9c2 cardiomyocytes

To further delineate the role of BMAL1 in cardiomyocytes under lipotoxic stress, H9c2 cells were assigned to four groups: CON-NC, PA-NC, PA-*Bmal1*-siRNA, and PA-*Bmal1*-AAV. This design enabled the evaluation of both loss- and gain-of-function effects of *Bmal1*, and the efficiency of *Bmal1* modulation was verified by immunoblotting and

densitometric analysis (***Supplementary Fig. 4A*** and ***4B***). To investigate the interplay among autophagosomes, lysosomes, and mitochondria under lipotoxic stress, we performed immunofluorescence labeling for LC3 (autophagosomes), LAMP1 (lysosomes), and TOM20 (mitochondria). PA treatment significantly increased mitochondria colocalization with both autophagosomes and lysosomes, indicating enhanced mitophagy (***Fig. 5A–5C***). This colocalization was further intensified upon *Bmal1* knockdown (PA-*Bmal1*-siRNA). TEM corroborated these findings, revealing that PA-*Bmal1*-siRNA treatment led to reduced mitochondrial number, pronounced vacuolization, and extensive mitochondrial cristae disruption (***Fig. 5D–5F*** and ***5H***). PA stimulation significantly increased autophagosome formation and mitophagy events compared with control conditions. *Bmal1* deficiency exacerbated mitophagy in cardiomyocytes, aggravating mitochondrial damage, whereas *Bmal1* overexpression reversed these pathological changes, restoring mitochondrial integrity and autophagy homeostasis (***Supplementary Fig. 4C*** and ***4D***).

FACS analysis demonstrated that PA stimulation significantly elevated the apoptosis rate compared with control, and this effect was exacerbated by *Bmal1* knockdown (***Fig. 5G*** and ***5I***). Under PA treatment, *Bmal1* deficiency further reduced ΔΨm (***Supplementary Fig. 4E***) and amplified mitochondrial ROS accumulation, indicating worsened mitochondrial dysfunction (***Supplementary Fig. 4F***).

Importantly, reconstitution of *Bmal1* expression *via* adenoviral delivery (PA-*Bmal1*-AAV) markedly reversed the deleterious effects of PA and *Bmal1* knockdown. *Bmal1* overexpression mitigated mitochondrial loss and morphological damage, suppressed autolysosome formation (***Fig. 5D–5H***), restored ΔΨm (***Supplementary Fig. 4E***), and reduced ROS buildup (***Supplementary Fig. 4F***).

Bmal1 alleviates lipid-induced mitophagy and is associated with reduced PINK1/Parkin signaling

Convergent transcriptomic and functional data consistently link *Bmal1* deficiency to activation of PINK1/Parkin-associated mitophagy under lipid stress. In obese mouse hearts, RNA-seq revealed marked upregulation of *Ambra1*, alongside coordinated downregulation of receptor/adapter genes (*Fundc1*, *Nbr1*, *Optn*, and *Tax1bp1*), suggesting suppression of alternative receptor-mediated routes (***Fig. 6A*** and ***6B***). The increase in AMBRA1 —an autophagy initiator that closely interacts with Parkin —points to a predominance of ubiquitin-dependent PINK1/Parkin signaling under this pathological state.

To explore the mechanistic link between *Bmal1* and mitochondrial autophagy under lipotoxic conditions, H9c2 cardiomyocytes were treated with increasing

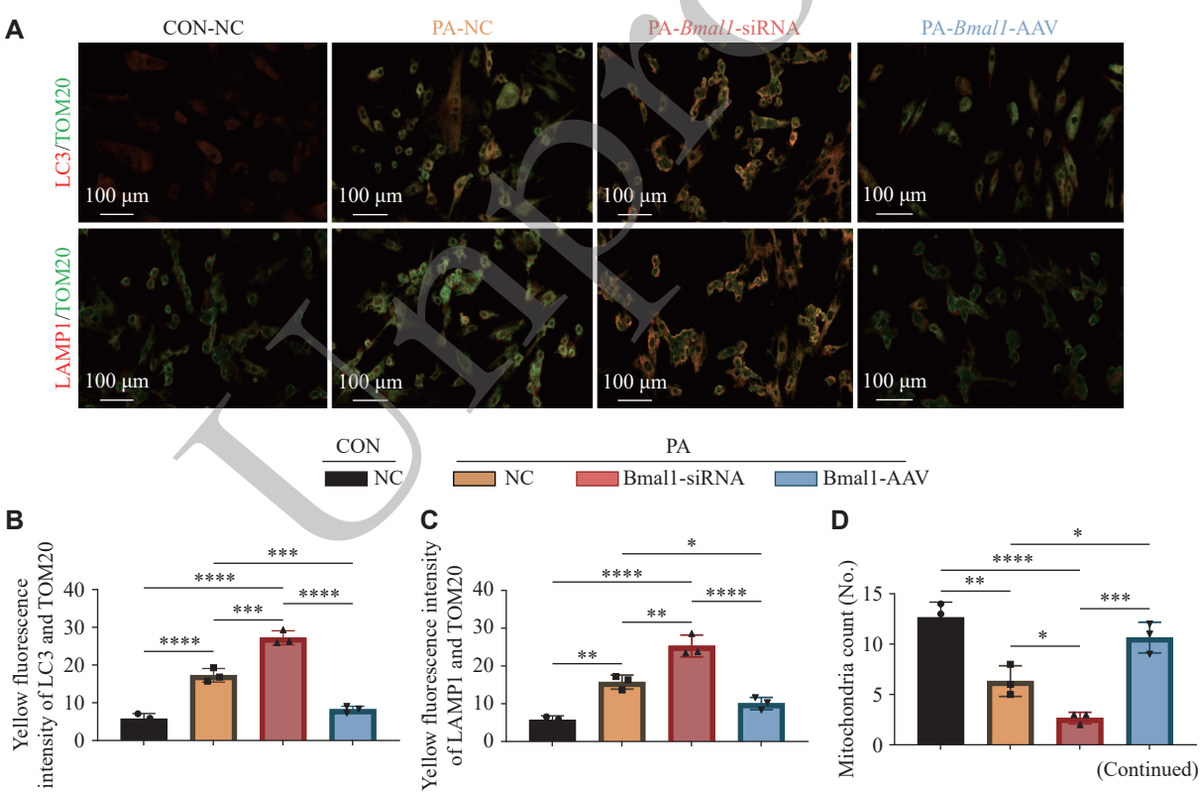

(Continued)

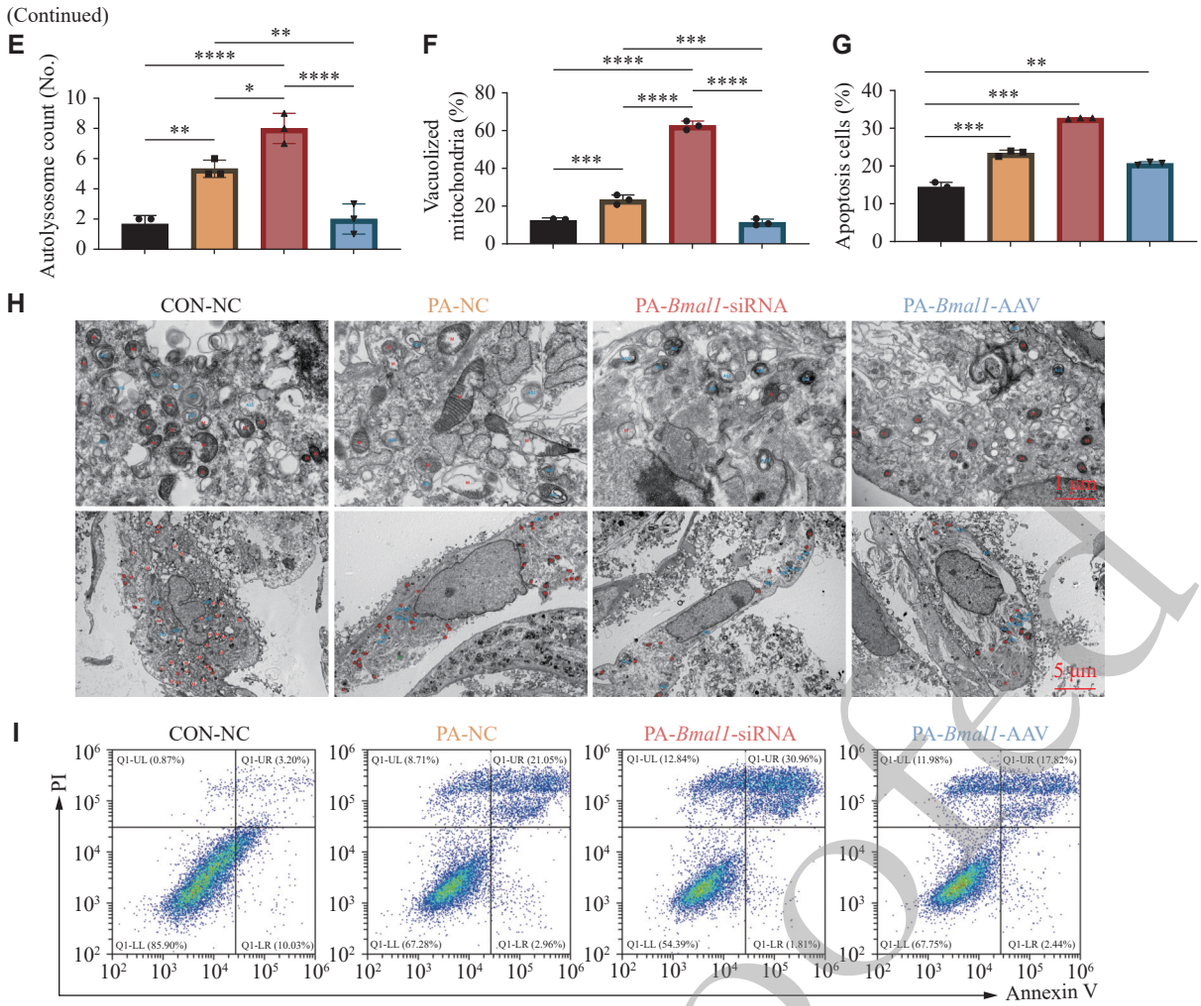

Fig. 5 **BMAL1 protects against palmitic acid (PA)-induced excessive mitophagy, mitochondrial damage, and apoptosis in cardiomyocytes.** A: Representative immunofluorescence images of H9c2 cells stained for LC3 (red), LAMP1 (red), TOM20 (green), and DAPI (blue) under four conditions: control (CON), palmitic acid (PA), PA with Bmal1 knockdown (PA-*Bmal1*-siRNA), and PA with Bmal1 overexpression (PA-*Bmal1*-AAV). Colocalization of LC3/TOM20 or LAMP1/TOM20 (yellow) indicates mitophagy activity. Scale bar, 100 μm. B:Quantification of LC3/TOM20 colocalization fluorescence intensity from (A) (n = 3 per group). C:Quantification of LAMP1/TOM20 colocalization fluorescence intensity from panel A (n = 3 per group). D: Mitochondrial count per field from TEM images (H) (*n* = 3 per group). E: Quantification of autolysosome count per field from TEM images (H) (*n* = 3 per group). F: Proportion of vacuolized mitochondria from TEM images (H) (*n* = 3 per group). G: Flow cytometry analysis of apoptosis rate (Annexin V/PI staining) (I) (*n* = 3 per group). H: Representative transmission electron microscopy (TEM) images showing mitochondrial ultrastructure and autolysosomes (blue/red asterisks). M indicates mitochondria and ASS indicate autolysosome. I: Flow cytometry scatter plots showing apoptosis under each condition. Data are presented as mean ± standard error (SD). ; each dot represents one mouse (biological replicate). For panels B–G, statistical analysis was performed using one-way ANOVA followed by Tukey's multiple-comparisons test. Statistical significance is indicated as *P < 0.05, **P < 0.01, ***P < 0.001, and ****P < 0.0001. Abbreviations: AAV, adeno-associated virus; CON, control; NC, negative control; PA, palmitic acid; siRNA, small interfering RNA; DAPI, 4′,6-diamidino-2-phenylindole; LAMP1, lysosome-associated membrane protein 1; LC3, microtubule-associated protein 1 light chain 3; PI, propidium iodide; TEM, transmission electron microscopy; TOM20, translocase of outer mitochondrial membrane 20.

concentrations of PA. A dose-dependent downregulation of *Bmal1* mRNA was observed, accompanied by concomitant upregulation of *Pink1* and *Parkin*, key regulators of mitophagy (***Fig. 6C*** and ***6D***). At the protein level, BMAL1 expression was markedly reduced under high-fat conditions, whereas PINK1 and Parkin levels were significantly elevated, indicating activation of the PINK1/Parkin-mediated mitophagy pathway (***Fig. 6E*** and ***6F***).

Notably, overexpression of *Bmal1 via* adenoviral transduction (PA-*Bmal1*-AAV) effectively reversed PA-induced activation of the PINK1/Parkin pathway, compared with vector controls (PA-Ctrl) (***Fig. 6G***). These results suggest that, under lipid overload, *Bmal1* downregulation and circadian disruption are associated with mitochondrial damage and enhanced mitophagy, accompanied by activation of the PINK1/Parkin signaling pathway.

Discussion

Our study identifies BMAL1, a core component of the molecular circadian clock, as a key regulator of myocardial homeostasis under obesity-induced stress. We demonstrate that obesity disrupts the rhythmic expression of *Bmal1* in the heart, leading to mitochondrial dysfunction, excessive mitophagy, and cardiomyocyte apoptosis (***Fig. 7***). Cardiac-specific deletion of *Bmal1* further exacerbates structural and functional deterioration, whereas *Bmal1* overexpression reverses these effects. *Bmal1* deficiency is associated with mitochondrial structural damage, enhanced mitophagy, and increased cardiomyocyte apoptosis, along with upregulation of PINK1/Parkin-related markers. Therefore, maintaining circadian rhythm homeostasis —particularly preserving BMAL1 function —may be

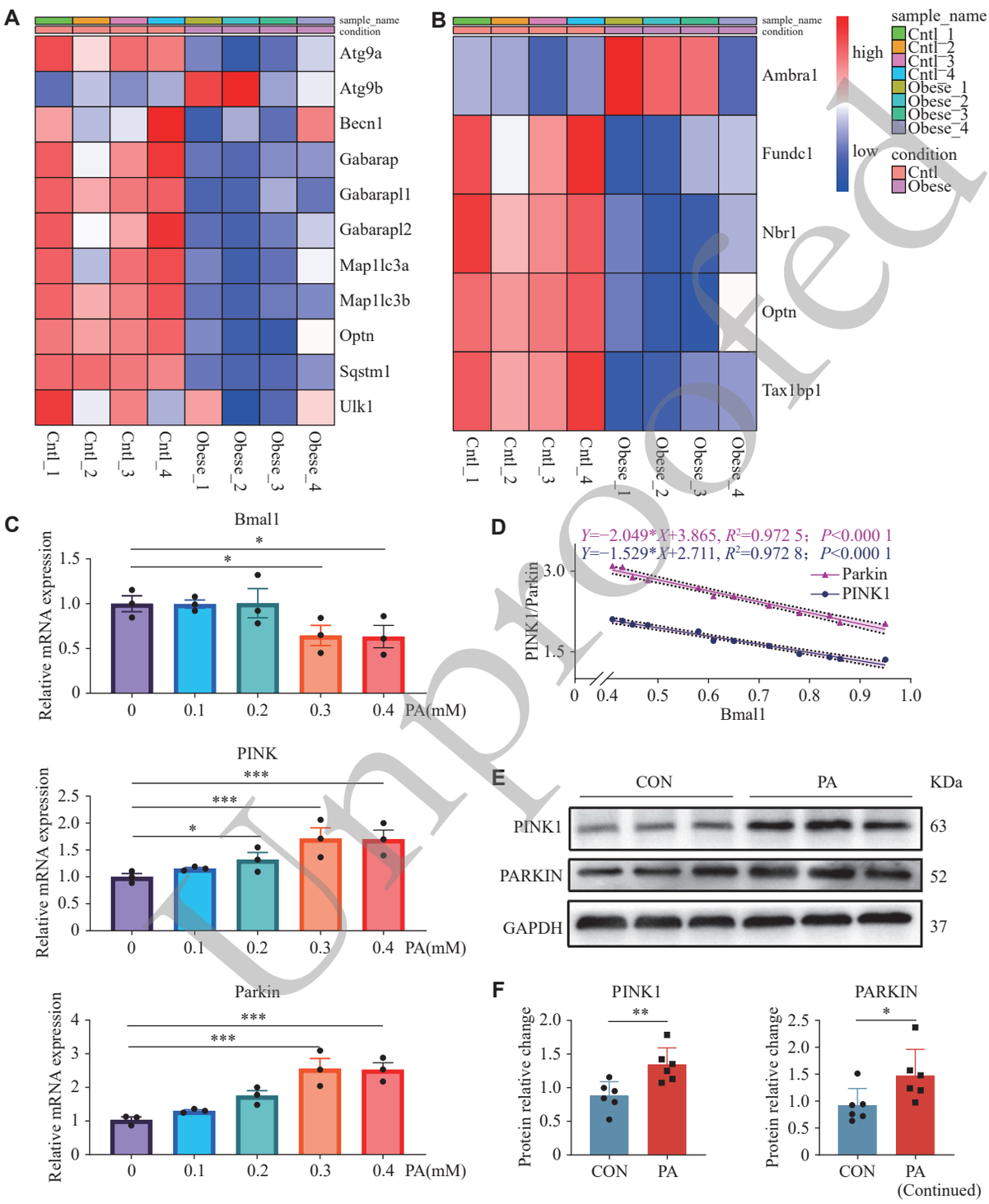

(Continued)

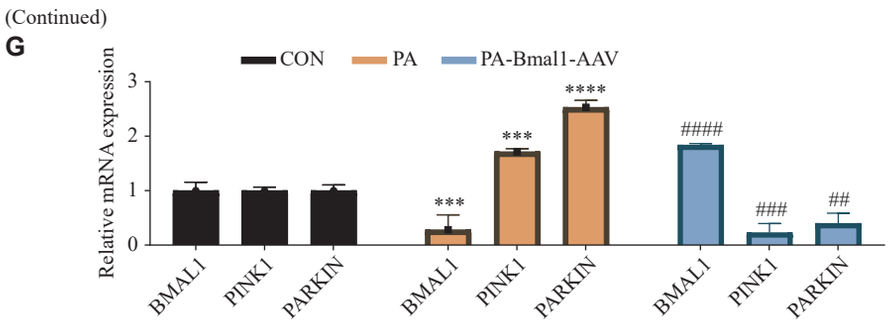

Fig. 6 **BMAL1 suppresses lipid-induced mitophagy by inhibiting the PINK1/Parkin pathway.** A: RNA-seq heatmap of autophagy-related genes in control and obese mouse hearts. Heatmap showing the normalized expression of representative autophagy genes across control (Ctrl) and obese heart samples. B: RNA-seq heatmap of *Ambra1* and mitophagy receptor/adaptor genes in control (Ctrl) and obese mouse hearts. C: qPCR analysis of mRNA levels of *Bmal1*, *Pink1*, and *Parkin* in H9c2 cardiomyocytes treated with increasing concentrations of palmitic acid (PA: 0, 0.1, 0.2, 0.4 mmol/L) for 24 h. (n = 3 per group). D: Pearson correlation analysis showed that *Bmal1* mRNA levels were negatively correlated with both *Pink1* and *Parkin* mRNA expression (n = 12). Each dot represents one sample; the solid line indicates the linear regression fit with 95% confidence intervals. E: Representative western blots of PINK1 and PARKIN in H9c2 cells cultured in standard medium (CON) or treated with PA (0.4 mmol/L) for 24 h. GAPDH served as a loading control. F: Quantification of PINK1 (E) and PARKIN (F) protein levels from (D), normalized to CON (n = 3). G: qPCR analysis of *Bmal1*, *Pink1*, and *Parkin* mRNA levels in H9c2 cells cultured in standard medium (CON), treated with PA (0.4 mmol/L) for 24 h (PA), or transduced with AAV-Bmal1 for 12 h followed by PA treatment (0.4 mmol/L) for 24 h (PA-Bmal1-AAV) (n = 3 per group). Data are presented as mean ± standard error (SD) ; each dot represents one mouse (biological replicate). For panels C and G, statistical analysis was performed using one-way ANOVA followed by Tukey's multiple-comparisons test. For panel D, Pearson correlation analysis was performed. For panel F, comparisons between two groups were performed using an unpaired two-tailed Student's t test. Statistical significance is indicated as $^{*}P < 0.05$, $^{**}P < 0.01$, $^{***}P < 0.001$, and $^{****}P < 0.0001$ vs. CON; $^{\#}P < 0.05$, $^{\#\#}P < 0.01$, and $^{\#\#\#}P < 0.001$ vs. PA.

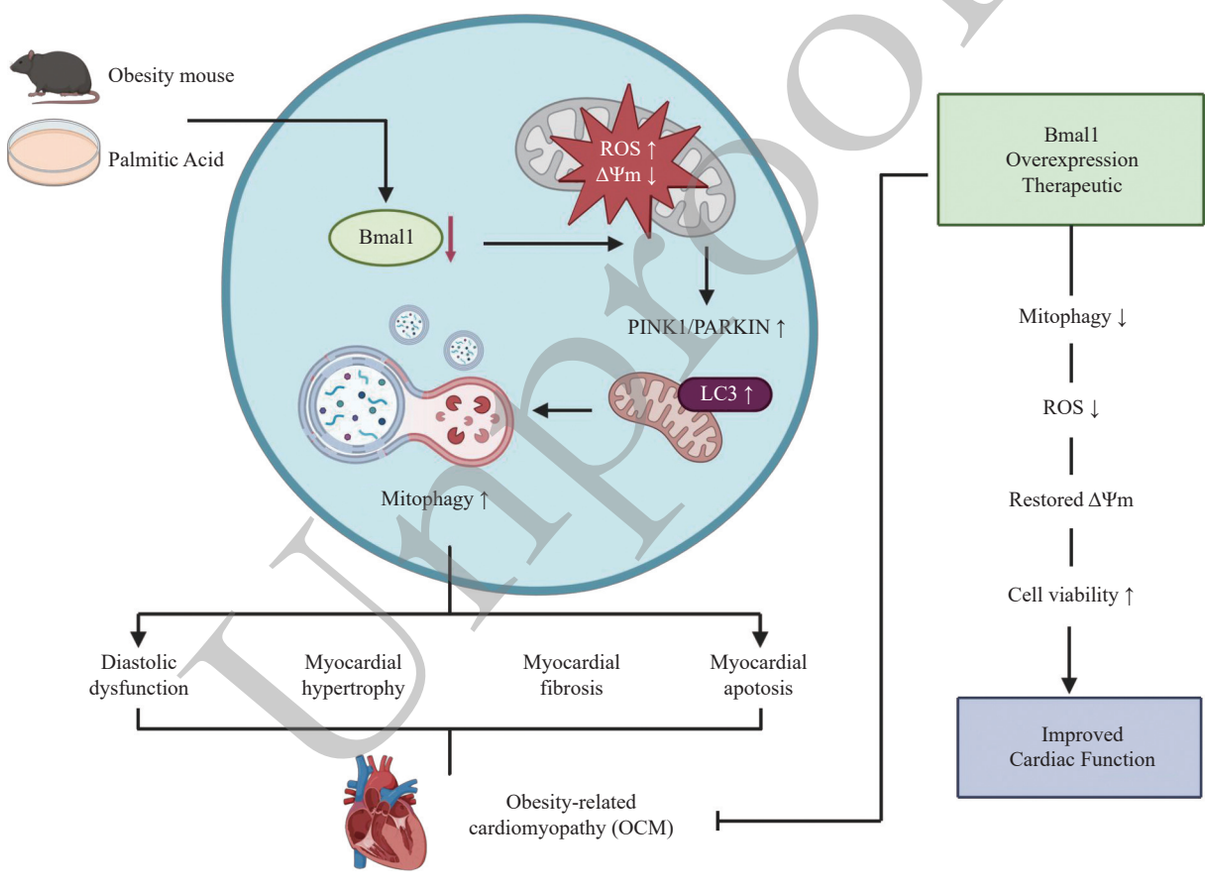

Fig. 7 **Proposed role of BMAL1 in obesity-related cardiomyopathy.** Schematic model illustrating that reduced BMAL1 expression under obesity-related metabolic stress may promote ROS accumulation, mitochondrial membrane potential decline, and PINK1/PARKIN-associated mitophagy in cardiomyocytes. These changes are linked to myocardial remodeling and impaired cardiac function, whereas BMAL1 overexpression exerts protective effects by suppressing excessive mitophagy and improving mitochondrial homeostasis.

beneficial for preventing or treating obesity-related cardiomyopathy.

The circadian clock system governs daily oscillations in cardiac metabolism, contractility, and gene expression. Our findings corroborate previous reports that HFD intake blunts or abolishes *Bmal1* rhythmicity in peripheral tissues, including the liver, skeletal muscle, and heart[22, 23]. The downregulation and arrhythmic expression of *Bmal1* observed in our HFD-fed mice suggest that metabolic overload can function as a zeitgeber that desynchronizes local cardiac clocks from the central suprachiasmatic nucleus[23]. Rhythmic *Bmal1* expression is essential for regulating genes involved in mitochondrial biogenesis, fatty acid oxidation, and antioxidant defense[24]. Loss of this rhythmic regulation may explain the increased cardiac lipid accumulation, fibrosis, and diastolic dysfunction observed in our obese mice. Moreover, we observed preserved systolic function despite extensive structural damage, consistent with the early stage of heart failure with preserved ejection fraction, commonly associated with metabolic syndrome[25].

Mitochondria are not only energy suppliers but also modulators of cell fate. Our study reveals that *Bmal1* deficiency aggravates mitochondrial dysfunction, characterized by reduced ΔΨm, increased mitochondrial ROS, and loss of mitochondrial mass. These features are hallmarks of intrinsic apoptotic signaling and are closely linked to cardiomyocyte death in lipotoxic cardiomyopathy. We show that *Bmal1* loss activates the PINK1/Parkin-mediated mitophagy pathway[26]. Under normal conditions, *Bmal1* inhibits excessive mitophagy to preserve mitochondrial content and energy supply[11, 27]. Prior studies indicate that BMAL1 regulates mitochondrial dynamics *via* direct transcriptional regulation of *Fis1*, *Mfn2*, and *Drp1*[28]. Our results extend this role by suggesting that *Bmal1* is associated with attenuated mitophagy and reduced *Pink1*/*Parkin* expression under lipid stress, consistent with observations reported in hepatocytes and neurons. Although mitophagy is essential for eliminating damaged mitochondria, its overactivation under chronic stress leads to mitochondrial depletion and an energetic crisis, ultimately promoting apoptosis[29]. Restoration of *Bmal1* in our *in vitro* model reversed mitochondrial loss and apoptosis, suggesting that BMAL1 acts as a gatekeeper of mitochondrial turnover under metabolic stress.

The therapeutic potential of targeting *Bmal1* is underscored by the efficacy of *Bmal1* overexpression in reversing PA-induced cardiomyocyte injury. Several studies support the notion that restoration of circadian gene expression improves cardiac resilience to metabolic insults. Pharmacological agents that amplify circadian amplitude or activate downstream targets of BMAL1 (*e.g.*, REV-ERB agonists and NAD^+ boosters) have shown promise in ameliorating metabolic disorders and cardiac dysfunction[30, 31]. Our findings not only provide mechanistic insight into the pathogenesis of obesity-related cardiac dysfunction but also identify a modifiable molecular target. Chronobiology-based strategies could complement current metabolic therapies and may be particularly beneficial for heart failure with preserved ejection fraction, a condition with limited treatment options in which inflammation, lipotoxicity, and mitochondrial dysfunction play dominant roles[32].

Several limitations warrant consideration. First, although H9c2 cells are widely used for cardiomyocyte research, they may not fully replicate the metabolic profile of adult primary cardiomyocytes. Future studies using human induced pluripotent stem cell-derived cardiomyocytes or adult mouse cardiomyocytes could enhance translational relevance[33]. Second, the roles of other mitophagy regulators, such as BNIP3, NIX, and FUNDC1, remain unexplored and should be investigated to delineate the broader regulatory network downstream of BMAL1[34]. Although we observed consistent changes in PINK1/Parkin expression and mitophagy/autophagy-related markers, mitophagy flux was not directly assessed. Future work employing dedicated flux assays will be important to determine whether the observed alterations reflect increased mitophagy activity or impaired downstream degradation. Moreover, while this study focused on male mice, sex-specific differences in circadian regulation and cardiac metabolism are increasingly recognized[35]. Female mice may exhibit different responses to *Bmal1* deletion or lipid overload, which should be addressed in future research. Lastly, clinical studies examining BMAL1 expression and circadian integrity in obese patients with early cardiac dysfunction could provide translational validation[13]. Interventional trials with circadian modulators will be necessary to establish therapeutic efficacy and safety.

In summary, our study demonstrates that BMAL1 plays a pivotal role in safeguarding cardiac structure and function under lipotoxic stress by maintaining mitochondrial homeostasis and suppressing excessive PINK1/Parkin-mediated mitophagy. Obesity-induced disruption of BMAL1 expression exacerbates mitochondrial dysfunction and apoptosis, thereby promoting the development of metabolic cardiomyopathy. Targeting the circadian machinery,

particularly BMAL1 and its downstream pathways, may offer novel therapeutic opportunities for the prevention and treatment of obesity-related heart disease.

Funding

This work was funded by the National Natural Science Foundation of China (Grant No. 81870251 to Jiangang Zou).

Author contributions

JGZ: Conceptualization, Writing —review & editing, Supervision, Project administration, Funding acquisition. **TZL:** Methodology, Formal analysis, Investigation, Data curation, Writing —review & editing. **XXF:** Methodology, Formal analysis, Investigation, Data curation, Writing—original draft, Writing—review & editing. **NNZ:** Formal analysis, Writing —review & editing. **YW:** Validation, Writing —review & editing. **ZYQ:** Validation, Writing —review & editing. **XFH:** Validation, Writing—review & editing. **HWZ:** Writing—review & editing.

Acknowledgments

None.

References

[1] GBD 2021 Adult BMI Collaborators. Global, regional, and national prevalence of adult overweight and obesity, 1990-2021, with forecasts to 2050: A forecasting study for the Global Burden of Disease Study 2021[J]. *Lancet*, 2025, 405(10481): 813–838.

[2] Powell-Wiley TM, Poirier P, Burke LE, et al. Obesity and cardiovascular disease: A scientific statement from the American Heart Association[J]. *Circulation*, 2021, 143(21): e984–e1010.

[3] Ren J, Wu NN, Wang S, et al. Obesity cardiomyopathy: Evidence, mechanisms, and therapeutic implications[J]. *Physiol Rev*, 2021, 101(4): 1745–1807.

[4] Kenchaiah S, Evans JC, Levy D, et al. Obesity and the risk of heart failure[J]. *N Engl J Med*, 2002, 347(5): 305–313.

[5] Tong M, Saito T, Zhai P, et al. Alternative mitophagy protects the heart against obesity-associated cardiomyopathy[J]. *Circ Res*, 2021, 129(12): 1105–1121.

[6] Jankauskas S, Kansakar U, De Donato A, et al. Parkin controls cardiac function in obesity by regulating mitochondrial calcium uptake[J]. *JACC Basic Transl Sci*, 2022, 7(8): 797–799.

[7] Shearman LP, Sriram S, Weaver DR, et al. Interacting molecular loops in the mammalian circadian clock[J]. *Science*, 2000, 288(5468): 1013–1019.

[8] Koike N, Yoo SH, Huang HC, et al. Transcriptional architecture and chromatin landscape of the core circadian clock in mammals[J]. *Science*, 2012, 338(6105): 349–354.

[9] Dunlap JC. Molecular bases for circadian clocks[J]. *Cell*, 1999, 96(2): 271–290.

[10] Zhang N, Yu H, Liu T, et al. Bmal1 downregulation leads to diabetic cardiomyopathy by promoting Bcl2/IP3R-mediated mitochondrial Ca^{2+} overload[J]. *Redox Biol*, 2023, 64: 102788.

[11] Li E, Li X, Huang J, et al. BMAL1 regulates mitochondrial fission and mitophagy through mitochondrial protein BNIP3 and is critical in the development of dilated cardiomyopathy[J]. *Protein Cell*, 2020, 11(9): 661–679.

[12] Schrader LA, Ronnekleiv-Kelly SM, Hogenesch JB, et al. Circadian disruption, clock genes, and metabolic health[J]. *J Clin Invest*, 2024, 134(14): e170998.

[13] Maury E, Navez B, Brichard SM. Circadian clock dysfunction in human omental fat links obesity to metabolic inflammation[J]. *Nat Commun*, 2021, 12(1): 2388.

[14] Xin H, Zhang J, Huang R, et al. Circadian signatures of adipose tissue in diet-induced obesity[J]. *Front Physiol*, 2022, 13: 953237.

[15] Tian R, Colucci WS, Arany Z, et al. Unlocking the secrets of mitochondria in the cardiovascular system: Path to a cure in heart failure-a report from the 2018 national heart, lung, and blood institute workshop[J]. *Circulation*, 2019, 140(14): 1205–1216.

[16] Bonora M, Wieckowski MR, Sinclair DA, et al. Targeting mitochondria for cardiovascular disorders: Therapeutic potential and obstacles[J]. *Nat Rev Cardiol*, 2019, 16(1): 33–55.

[17] Ravindran S, Rau CD. The multifaceted role of mitochondria in cardiac function: Insights and approaches[J]. *Cell Commun Signal*, 2024, 22(1): 525.

[18] Yancy CW, Jessup M, Bozkurt B, et al. 2017 ACC/AHA/HFSA focused update of the 2013 ACCF/AHA guideline for the management of heart failure: A report of the American College of Cardiology/American Heart Association task force on clinical practice guidelines and the heart failure society of America[J]. *Circulation*, 2017, 136(6): e137–e161.

[19] Tong M, Saito T, Zhai P, et al. Mitophagy is essential for maintaining cardiac function during high fat diet-induced diabetic cardiomyopathy[J]. *Circ Res*, 2019, 124(9): 1360–1371.

[20] Morales PE, Arias-Durán C, Ávalos-Guajardo Y, et al. Emerging role of mitophagy in cardiovascular physiology and pathology[J]. *Mol Aspects Med*, 2020, 71: 100822.

[21] Shires SE, Gustafsson ÅB. Mitophagy and heart failure[J]. *J Mol Med (Berl)*, 2015, 93(3): 253–262.

[22] Kohsaka A, Laposky AD, Ramsey KM, et al. High-fat diet disrupts behavioral and molecular circadian rhythms in

mice[J]. *Cell Metab*, 2007, 6(5): 414–421.

[23] Jang H, Lee G, Kong J, et al. Feeding period restriction alters the expression of peripheral circadian rhythm genes without changing body weight in mice[J]. *PLoS One*, 2012, 7(11): e49993.

[24] Dyar KA, Hubert MJ, Mir AA, et al. Transcriptional programming of lipid and amino acid metabolism by the skeletal muscle circadian clock[J]. *PLoS Biol*, 2018, 16(8): e2005886.

[25] Van Laake LW, Lüscher TF, Young ME. The circadian clock in cardiovascular regulation and disease: Lessons from the Nobel Prize in Physiology or Medicine 2017[J]. *Eur Heart J*, 2018, 39(24): 2326–2329.

[26] Lin Q, Chen J, Gu L, et al. New insights into mitophagy and stem cells[J]. *Stem Cell Res Ther*, 2021, 12(1): 452.

[27] Jacobi D, Liu S, Burkewitz K, et al. Hepatic bmal1 regulates rhythmic mitochondrial dynamics and promotes metabolic fitness[J]. *Cell Metab*, 2015, 22(4): 709–720.

[28] de Goede P, Wefers J, Brombacher EC, et al. Circadian rhythms in mitochondrial respiration[J]. *J Mol Endocrinol*, 2018, 60(3): R115–R130.

[29] Jin Z, Ji Y, Su W, et al. The role of circadian clock-controlled mitochondrial dynamics in diabetic cardiomyopathy[J]. *Front Immunol*, 2023, 14: 1142512.

[30] Wang P, Yu B, Liu L, et al. Role of circadian rhythms in heart failure: Insights from myocardial energy metabolism[J]. *J Transl Med*, 2025, 23(1): 770.

[31] Li H, Song S, Tien CL, et al. SR9009 improves heart function after pressure overload independent of cardiac REV-ERB[J]. *Front Cardiovasc Med*, 2022, 9: 952114.

[32] Lal H, Verma SK, Wang Y, et al. Circadian rhythms in cardiovascular metabolism[J]. *Circ Res*, 2024, 134(6): 635–658.

[33] Wang PH, Fang YH, Liu YW, et al. Merits of hiPSC-derived cardiomyocytes for in vitro research and testing drug toxicity[J]. *Biomedicines*, 2022, 10(11): 2764.

[34] Lampert MA, Orogo AM, Najor RH, et al. BNIP3L/NIX and FUNDC1-mediated mitophagy is required for mitochondrial network remodeling during cardiac progenitor cell differentiation[J]. *Autophagy*, 2019, 15(7): 1182–1198.

[35] Zhang X, Procopio SB, Ding H, et al. The core circadian clock factor, *Bmal1*, transduces sex-specific differences in both rhythmic and nonrhythmic gene expression in the mouse heart[J]. *Function (Oxf)*, 2025, 6(1): zqae053.